Quantification of the novel N-methyl-D-aspartate receptor ligand [11C]GMOM in man

**Thalia F van der Doef[1,2]*, Sandeep SV Golla[1]*, Pieter J Klein[1],
Gisela M Oropeza-Seguias[1], Robert C Schuit[1],
Athanasios Metaxas[1], Ellen Jobse[1], Lothar A Schwarte[3],
Albert D Windhorst[1], Adriaan A Lammertsma[1],
Bart NM van Berckel[1,2] and Ronald Boellaard[1]**

Abstract

[11C]GMOM (carbon-11 labeled N-(2-chloro-5-thiomethylphenyl)-N′-(3-[11C]methoxy-phenyl)-N′-methylguanidine) is a PET ligand that binds to the N-methyl-D-aspartate receptor with high specificity and affinity. The purpose of this first in human study was to evaluate kinetics of [11C]GMOM in the healthy human brain and to identify the optimal pharmacokinetic model for quantifying these kinetics, both before and after a pharmacological dose of S-ketamine. Dynamic 90 min [11C]GMOM PET scans were obtained from 10 subjects. In six of the 10 subjects, a second PET scan was performed following an S-ketamine challenge. Metabolite corrected plasma input functions were obtained for all scans. Regional time activity curves were fitted to various single- and two-tissue compartment models. Best fits were obtained using a two-tissue irreversible model with blood volume parameter. The highest net influx rate (K_i) of [11C]GMOM was observed in regions with high N-methyl-D-aspartate receptor density, such as hippocampus and thalamus. A significant reduction in the K_i was observed for the entire brain after administration of ketamine, suggesting specific binding to the N-methyl-D-aspartate receptors. This initial study suggests that the [11C]GMOM could be used for quantification of N-methyl-D-aspartate receptors.

Introduction

N-methyl-D-aspartate (NMDA) receptors belong to a family of ligand-gated ionotropic channels. NMDA receptors are important sites of action for glutamate, the major excitatory neurotransmitter of the central nervous system. These receptors are tetramer complexes incorporating NR1, NR2, and NR3 subunits, and each subunit may have its own variations. This, in turn, results in a variety of different NMDA receptor compositions, each with its own characteristic pharmacological properties.[1,2] NMDA receptor activation requires binding of glutamate and either glycine or D-serine to their respective binding sites. Once the NMDA receptor is activated, its cation channel opens

[1]Department of Radiology & Nuclear Medicine, VU University Medical Center, Amsterdam, The Netherlands
[2]Department of Psychiatry, University Medical Center Utrecht, Utrecht, The Netherlands
[3]Department of Anesthesiology, VU University Medical Center, Amsterdam, The Netherlands

*Both authors contributed equally to this work

Corresponding author:
Sandeep SV Golla, VU University Medical Center, Department of Radiology & Nuclear Medicine, De Boelelaan 1117, 1081 HV Amsterdam, The Netherlands.
Email: s.golla@vumc.nl

allowing the passage of calcium, sodium, and potassium ions. Phencyclidine (PCP) and other psychoactive drugs, such as ketamine and dizocilpine (MK-801), bind to their target site, which is located within the cation channel of the NMDA receptor.[3,4]

The NMDA receptor has widespread expression in the central nervous system and it is involved in many biological functions, including brain development, synaptic plasticity, and cognitive processes such as memory and learning.[1,5] Alterations in both NMDA receptor composition and function have been implicated in a wide range of neurological and psychiatric diseases such as Alzheimer's disease (AD), Parkinson's disease and Huntington's disease, addiction disorders, and schizophrenia.[6,7] Pharmaceuticals acting on the NMDA receptor, such as the partial NMDA antagonist memantine, are approved for treatment of AD within the U.S. and Europe.[8] Imaging the NMDA receptor with positron emission tomography (PET) would provide useful information on the role of the NMDA receptor in the pathophysiology of these diseases.

Several candidate PET and single photon emission computerized tomography (SPECT) radioligands have been synthesized as potential imaging agents for the NMDA receptor. Most of these ligands, however, have failed due to either high nonspecific binding, poor metabolic stability, or insufficient affinity.[2,9] [123I]CNS 1261 and [11C]GMOM have shown the most promising preclinical results.[2,10] [11C]CNS 5161 has been tested in vivo in the human brain but quantification was difficult due to fast metabolism and low radiochemical yield.[11,12] Recently, a Fluorine-18 labeled analog of [11C]CNS 5161, [18F]GE-179 has been proposed as a putative NMDA receptor ligand, based on its high brain uptake in healthy volunteers.[12] This tracer also binds to the PCP site of the NMDA receptor, just like other diarylguanidines.[9] However, McGinnity et al.[12] concluded that further evaluation of [18F]GE-179 was needed to assess its in vivo specificity. In other words, there is still a need to evaluate alternative specific tracers of the NMDA receptor.

In nonhuman primate studies, [11C]GMOM showed high uptake and was able to demonstrate changes in modulation of NMDA ion channel activity by MK801.[13] Consequently, [11C]GMOM may have potential for in vivo quantification of the NMDA receptor in humans. The purpose of the present study was to evaluate [11C]GMOM in vivo in the human brain with the primary aim to identify the most appropriate kinetic model for quantification of [11C]GMOM binding in healthy volunteers. Moreover, blocking studies were performed to provide insight in the feasibility of studying [11C]GMOM binding in the presence of a pharmacological challenge.

Materials and methods

Subjects

Ten healthy volunteers with an age ranging from 20 to 28 years (mean age 23 years; 9 men, 1 woman) participated in this study. All subjects were free of medical and psychiatric illnesses based on medical history, neurological examination, blood tests (complete blood count and serum chemistry), urine analysis, and urine toxicology. The study was approved by the Medical Ethical Review Committee of the VU University Medical Center. All subjects provided written informed consent after complete explanation of the study procedures.

Radiochemistry

[11C]GMOM was synthesized using an adaptation of the method of Waterhouse.[13] Radiochemical purity (95.0–99.3%) with no detectable UV impurities was obtained. Yields were 1470–5560 MBq at end of synthesis (3–11%, not corrected for decay) and the specific activity (SA) was 97–288 GBq μmol^{-1} at end of synthesis. The product was sterile and pyrogen free and manufactured under GMP license NL/H11/0005, issued by the national competent authorities. A specific activity of 77 ± 37 GBq μmol^{-1} and a radioactivity concentration of 391 ± 8 MBq [11C]GMOM at the time of injection was produced.

PET

PET scans were performed on a Gemini TF-64 PET/CT scanner (Philips Medical Systems, Cleveland, OH, USA).[14] All ten subjects underwent [11C]GMOM scans at baseline, and six of them also with a second scan after an S-ketamine challenge. After a bolus injection of 391 ± 8 MBq [11C]GMOM, a 90 min dynamic PET scan was acquired. In addition, a low-dose CT (20 mAs, 80 kVp) was obtained for attenuation correction. Emission data were reconstructed into 22 frames (1×15, 3×5, 3×10, 4×60, 2×150, 2×300, 7×600 s) using a three-dimensional row action maximum likelihood reconstruction algorithm,[14,15] including data normalization and corrections for dead time, randoms, scatter, attenuation, and decay.

As mentioned above, six of the 10 subjects (5 M, 1 F, 22 ± 2 years) had two dynamic [11C]GMOM scans on the same day, a baseline scan in the morning followed by a challenge scan in the afternoon. There were no observed significant differences in mean injected dose of [11C]GMOM between baseline and challenge scans (dose baseline: 387 ± 8 MBq, dose challenge: 375 ± 10 MBq, $p = 0.92$, Wilcoxon signed-rank test), nor in SA at time of injection (SA baseline: 62 ± 30 GBq μmol^{-1},

SA challenge $60 \pm 19\,\mathrm{GBq\,\mu mol}^{-1}$, p $= 0.08$, Wilcoxon signed-rank test). The minimum time interval between both scans was 4 h.

S-ketamine challenge

S-ketamine was administered intravenously $(0.3\,\mathrm{mgkg}^{-1})$ in a pseudo-steady state model with a sub-acute loading dose. This dose is specific for the NMDA receptor as its analgesic effects are not blocked by naltrexone, a µ-opioid antagonist.[16,17] First, S-ketamine was administered in a 40 min initial phase $(0.004\,\mathrm{mgkg}^{-1}\mathrm{min}^{-1})$ followed by a 10 min adjustment phase $(0.0026\,\mathrm{mgkg}^{-1}\mathrm{min}^{-1})$. [11C]GMOM was injected immediately after the adjustment phase. Subsequently, administration of S-ketamine $(0.0013\,\mathrm{mgkg}^{1}\mathrm{min}^{-1})$ continued for a period of 85 min in the equilibrium phase.

Based on the mean plasma levels of S-ketamine measured during the blocking scans ($56.2\,\mathrm{ngml}^{-1}$; molecular weight: $237.725\,\mathrm{g\,mol}^{-1}$) and an apparent affinity value of $\sim 1\,\mu M$ for S-ketamine against [3H]MK-801 (K_i), an approximate occupancy value of the NMDA receptor ion-channel by S-ketamine throughout the study would be $\sim 19\%$ ([Conc]/[Conc]+K_D). Our calculations assume that S-ketamine distributes evenly in plasma and the brain and does not take into account binding to plasma proteins.

Input function

During the [11C]GMOM scan, the whole blood radioactivity concentration was measured continuously using an online blood sampler detection system (Veenstra Instruments, Joure, The Netherlands).[18] The withdrawal rate was $5\,\mathrm{ml\,min}^{-1}$ during the first 5 min, followed by $2.5\,\mathrm{ml\,min}^{-1}$ until 65 min postinjection (p.i.). At seven time points (5, 10, 20, 40, 60, 75, 85 min p.i.), continuous blood withdrawal was interrupted briefly to allow for collection of manual arterial blood samples (10 ml). Following each sample, the cannula was flushed with heparinized saline to prevent clotting. The manual samples were used to measure plasma to whole blood (P/WB) radioactivity ratios, and radioactive fractions of [11C]GMOM and its radioactive metabolites in plasma.

Plasma samples were analyzed using solid-phase extraction combined with HPLC using off-line radioactivity detection.[19] Three fractions were determined: [11C]GMOM, nonpolar metabolites, and polar metabolites. One minus the polar fraction was used as a surrogate for the parent fraction, as estimation of intact [11C]GMOM was not robust due to fast metabolism and the amount of nonpolar metabolites was very small and unreliable ($1.5 \pm 2.0\%$ at 90 min p.i.).

Each plasma input function was corrected for blood-to-plasma ratio, (polar) metabolites, and time delay. The manual arterial blood samples were also used for determining the S-ketamine concentration in plasma. These sample calculations were performed in duplicate. The area under the S-ketamine concentration–time curve was estimated by means of the trapezoidal rule.

Regions of interest (ROI) delineation

For anatomical delineation of ROIs, a structural magnetic resonance image (MRI) was obtained on a 1.5 T Sonata scanner (Siemens Medical Solutions, Erlangen, Germany). Scanning included a coronal T1-weighted scan (echo time 3.97 ms, repetition time 2700 ms, flip angle 8°, 160 coronal slices, voxel size $1.0 \times 1.5 \times 1.0\,\mathrm{mm}^3$). T1-weighted MRIs were co-registered to an average PET image (5–16 frames) using VINCI software.[20] The co-registered MRIs were segmented into gray matter, white matter, and extra-cerebral fluid, and regional time activity curves (TACs) were extracted using PVE-lab.[21–23] For the present study, eight ROIs were redefined by combining the ROIs extracted from the PVE-lab. The selection of ROIs was based on the widespread NMDA receptor availability in the brain: frontal, temporal, occipital, and parietal cortex, hippocampus, thalamus, striatum, and cerebellum, as well as whole brain gray matter.

Kinetic modeling

A total of seven compartment models were evaluated: standard singe-tissue (1T2k), irreversible (2T3k), and reversible (2T4k) two-tissue compartmental models, both with and without an additional (fit-)parameter for fractional blood volume (V_B). In addition, a dual input compartmental model (D1T2k) with blood volume fraction (fit-)parameter was included to evaluate the possibility that polar metabolites enter the brain and have impact on the kinetics observed. Effects of scan duration on model preference were tested by repeating the procedure mentioned above for the initial 60, 50, and 40 min of scan data.

Statistics

The optimal tracer kinetic model for describing [11C]GMOM kinetics was determined using the Akaike information criterion (AIC).[24] The nonparametric Wilcoxon signed-rank test without multiple corrections was used to assess whether there were significant differences in pharmacokinetic parameters (estimated from the preferred model) between baseline and S-ketamine scans. To calculate the significance of the postketamine decrease in Ki at the level of the whole
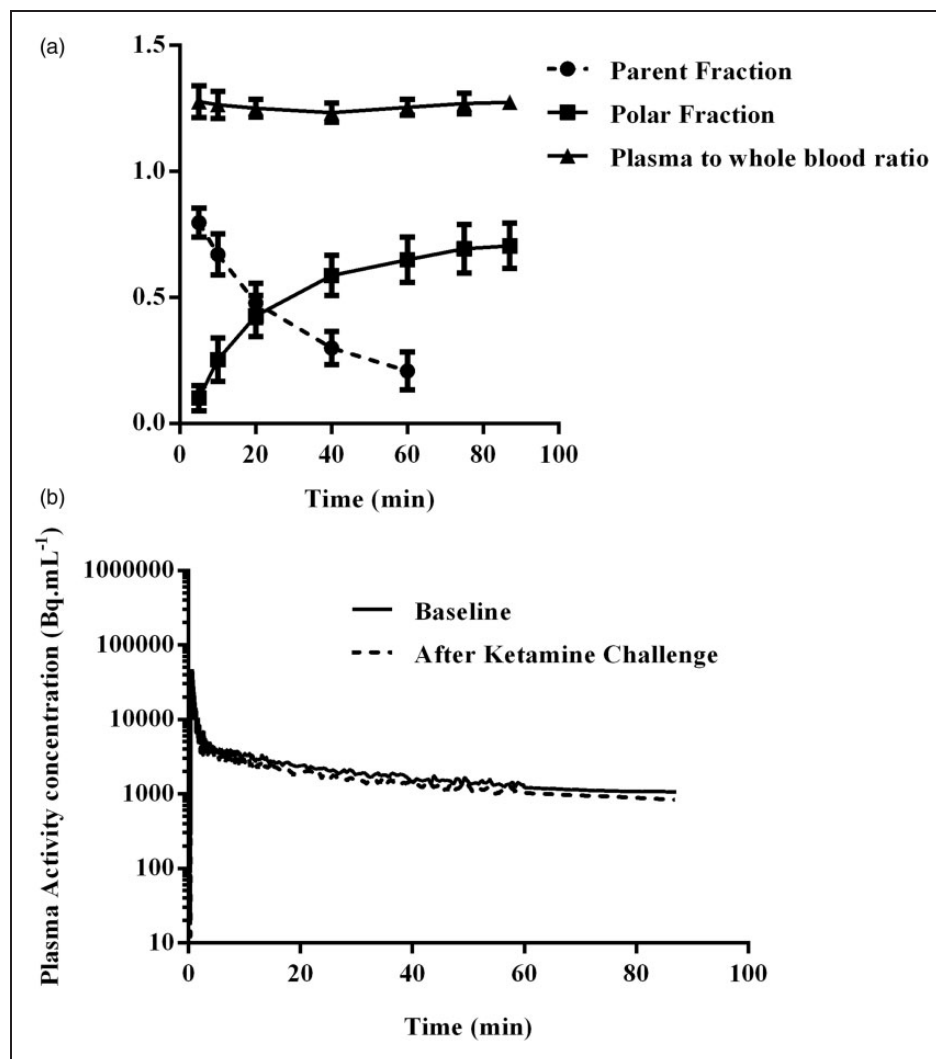
Figure 1. (a) Mean (± SD) of parent, polar fractions, and plasma to whole blood ratios for all available scans (N = 15), parent fractions for 75 and 90 min could not be measured. (b) Typical metabolite corrected plasma input functions (Y-axis, logarithmic scale) for baseline and S-ketamine challenge scans.

brain, linear mixed effect modeling was performed using SPSS software, and considering regions, patients, and conditions (i.e. before and after challenge) as factors. In this statistical test, regions and conditions were considered as fixed and patients as random factors, respectively. For all analyses, $p < 0.05$ was considered to be significant and $0.05 < p < 0.1$ as a trend level.

Results

Input function and plasma metabolite analysis

Figure 1(a) shows the average (±SD) parent fractions, polar fractions, and plasma to whole blood ratios for all available scans (N = 15). [^{11}C]GMOM has fairly rapid metabolism, which is shown by the fast decrease in parent fraction from 0.80 ± 0.06 at 5 min p.i. to

0.21 ± 0.08 at 60 min p.i. Parent fractions at the last two time points (75 and 90 min p.i.) were too small for reliable estimates. There were no significant differences in tracer metabolism between baseline and S-ketamine scans as indicated by the Wilcoxon signed-rank test. One pair out of the six paired baseline and ketamine challenge scans was excluded from this statistical analysis due to technical problems encountered during metabolite analysis for one of the scans (baseline scan). Input functions of baseline and ketamine challenge scans for a typical subject are illustrated in Figure 1(b) and Supplementary Figure 1.
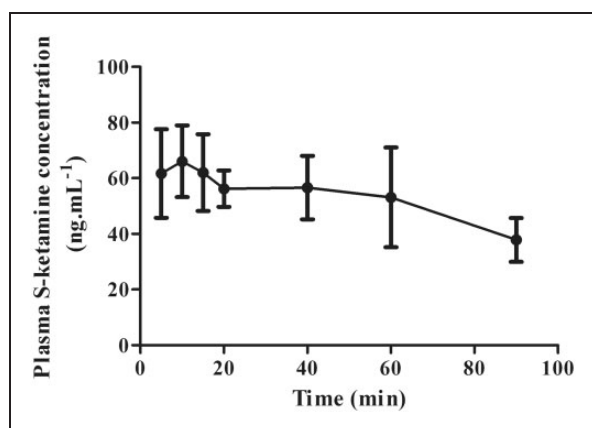
S-ketamine

S-ketamine was administered in a pseudo-steady state. During scans subjects were able to tolerate the

administered S-ketamine dose. Mean S-ketamine concentrations of the six subjects started at 62 ng ml^{-1} at 5 min p.i. and decreased to 38 ng ml^{-1} at the end of the scan (Figure 2).

ROI data analysis

A representative example of [^{11}C]GMOM brain uptake in a healthy volunteer is provided in Figure 3. Similar to the known expression of NMDA, a whole brain activity distribution was observed. Lower brain activity is seen after the S-ketamine challenge than in the baseline condition at all-time points p.i. (Figure 3). Figure 4 shows typical TACs corrected for injected activity (%ID ml^{-1}) from the eight ROIs and whole brain gray matter. Radioactivity concentrations were highest

Figure 2. Mean (±SD) plasma levels of S-ketamine in six healthy volunteers after intravenous administration of 0.3 mg kg^{-1} S-ketamine in a pseudo-steady state manner.

in thalamus and striatum, both at baseline and after S-ketamine.

Kinetic modeling

A total of 15 scans (nine baseline, six S-ketamine) were used to identify the optimal kinetic model. Figure 5 illustrates that the irreversible two-tissue compartment model with blood volume parameter (2T3k_V$_B$) was the preferred model based on AIC. Less preference was observed for the dual input model with blood volume fraction parameter (D1T2k_V$_B$). There was no difference in model preference between baseline and S-ketamine scans. In addition, after separating ROIs in small (<2 ml), medium (2–5 ml), and large (>5 ml) ones, no effect of region size on model preference was seen. All regions fitted best to the 2T3k_V$_B$ model, although this preference was most prominent for large regions.

With decreasing scan duration, model preference slowly shifted toward the reversible single-tissue model with additional blood volume parameter (1T2k_V$_B$). For the majority of ROIs, the 2T3k_V$_B$ was still preferred in case of 60 min datasets. For the 50 min datasets, however, there was equal preference for 1T2k_V$_B$ and 2T3k_V$_B$ models, and for the 40 min dataset the 1T2k_V$_B$ was preferred.

Since 2T3k_V$_B$ was the preferred model, the primary outcome parameter was the net influx rate constant K$_i$ (K$_i$ = (K$_1$·k$_3$)/(k$_2$ + k$_3$)). K$_i$ values were compared between baseline and S-ketamine challenge scans in order to determine the specific signal of [^{11}C]GMOM for the NMDA receptor. Mean nondisplaceable distribution volumes (V$_{ND}$ = K$_1$/k$_2$) of baseline and challenge conditions were compared to assess the effect on
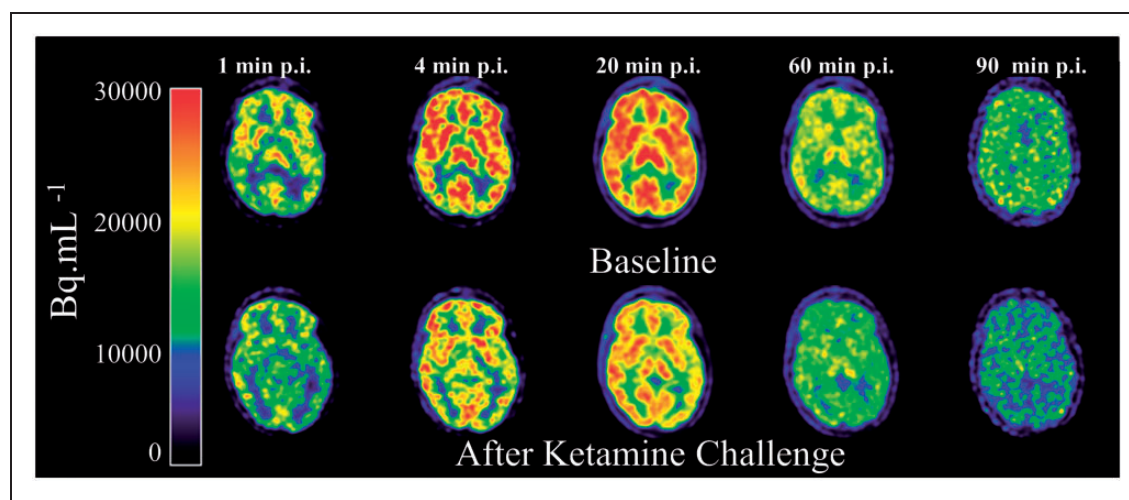
Figure 3. Transaxial image of [^{11}C]GMOM uptake (Bq ml^{-1}) in a healthy volunteer at different times postinjection (p.i.), at baseline (top) and after S-ketamine challenge (bottom).
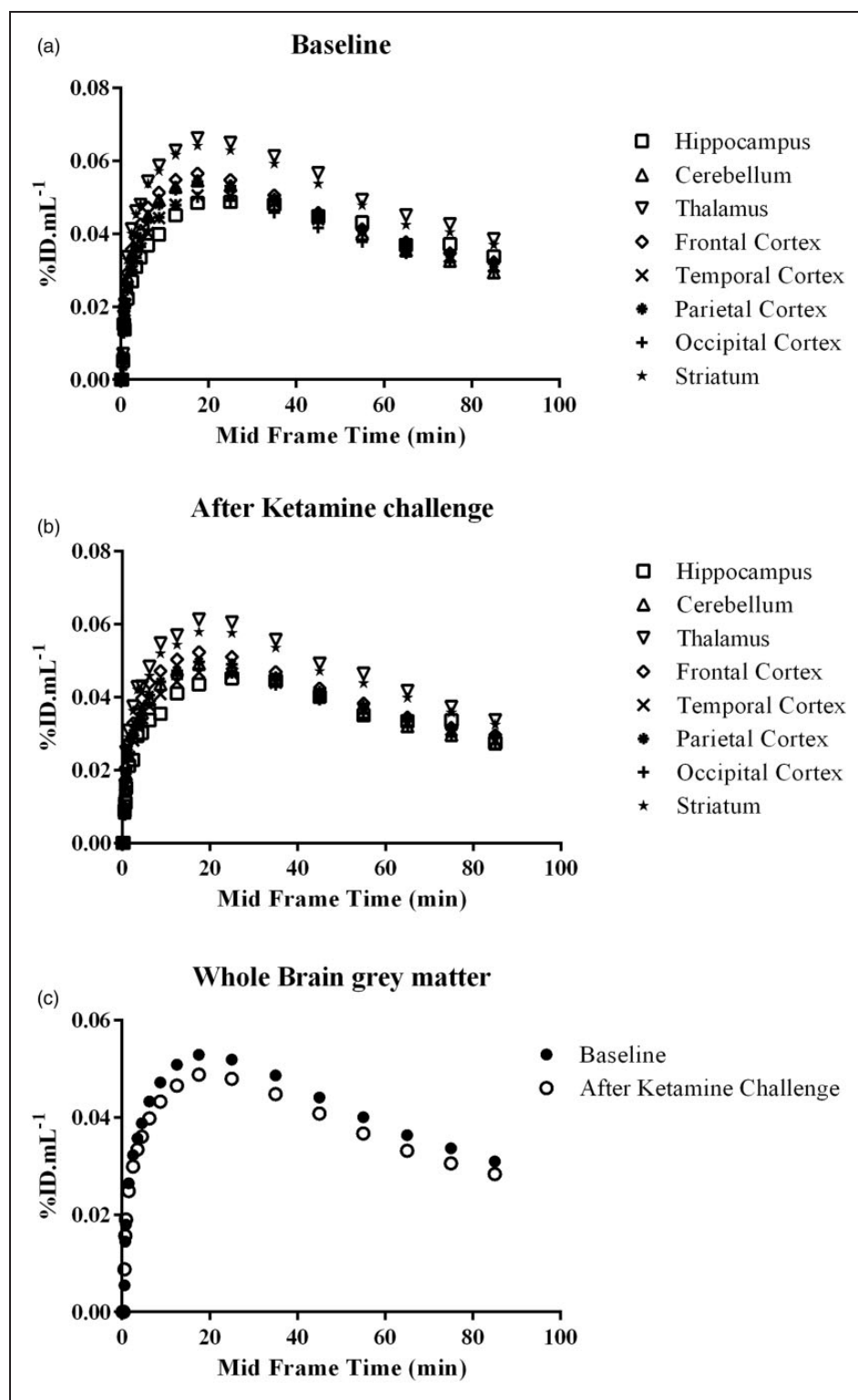
Figure 4. Time activity curves (TACs) corrected for injected activity (%ID mL^{-1}) from selected regions: hippocampus, thalamus, striatum, cerebellum, frontal, temporal, parietal and occipital cortex, for a typical subject (a) at baseline, (b) after S-ketamine, and (c) from whole brain gray matter at baseline and after S-ketamine.
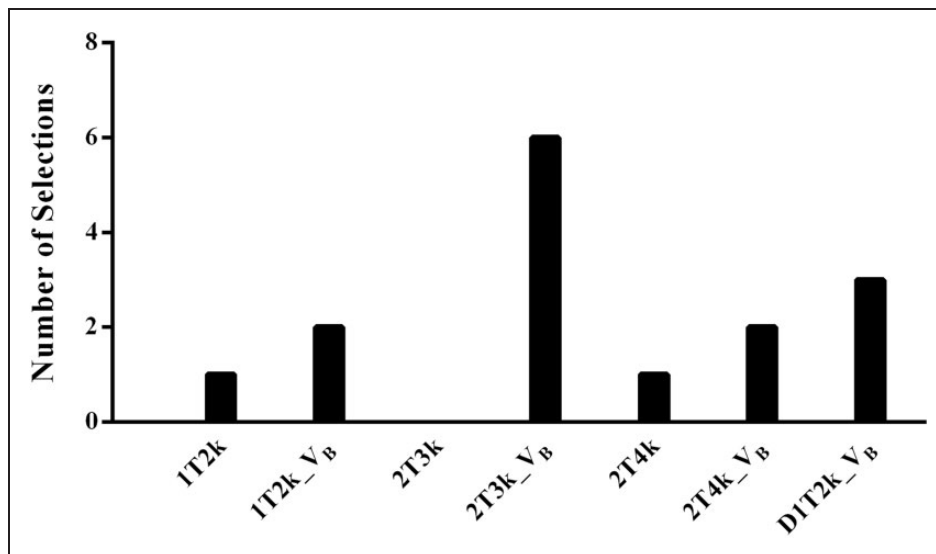
Figure 5. Number of preferred fits (y-axis) per model (x-axis) according to AIC for the 90 min datasets.

the nondisplaceable compartment. In addition, potential differences in mean rate constant K_1 between baseline and S-ketamine data were investigated to assess whether S-ketamine had an effect on the influx of $[^{11}C]$GMOM. Results obtained using the 2T3k_V_B model are summarized in Table 1. Baseline K_i values were highest in hippocampus and thalamus, followed by frontal, parietal and occipital cortex, striatum, temporal cortex, and cerebellum (Table 1). Figure 6 shows differences in K_i values for all ROIs averaged between baseline (N = 9) and S-ketamine (N = 6) scans.

After S-ketamine challenge, a significant decrease in K_i (linear mixed effects models, factors are ROI, patient and condition (before and after challenge), p < 0.0001) was observed at the whole brain level. The linear mixed effects model showed no interaction between ROI and condition, suggesting that all considered ROIs showed a similar change in K_i (Figure 6). It should be noted that, after S-ketamine administration, K_i values increased in one of the subjects (>75% for all ROI), but no reason for this unexpected observation could be found. When excluding this outlier, the percentage change in the mean K_i of total brain gray matter was $-66 \pm 23\%$ and, in thalamus and hippocampus of $-79 \pm 24\%$ and $-70 \pm 12\%$, respectively.

No significant difference in V_{ND} was observed in whole brain gray matter (Wilcoxon signed-rank test, p = 0.14), as well as in most other ROIs. Nevertheless, a significant increase in V_{ND} in the S-ketamine condition was found in cerebellum and hippocampus (Wilcoxon signed-rank test, p = 0.04). Similar results when excluding the outlier was observed, however with more regions showing a significant increase in the V_{ND}. The mean rate of transport K_1 ranged from

0.36 to 0.52 mlcm^{-3}min^{-1}, reflecting high extraction of $[^{11}C]$GMOM. No significant differences in K_1 were found between baseline and S-ketamine scans for all ROIs both including or excluding the outlier (Table 1). On performing linear mixed effects model analysis for V_{ND} and K_1, a significant but small increase (10% for V_{ND} and 7% for K_1) after the challenge was observed.

Discussion

To the best of our knowledge, this is the first study assessing the potential of $[^{11}C]$GMOM for in vivo quantification of NMDA receptors in the human brain. Results indicate that the irreversible two-tissue compartment model with additional fractional blood volume (fit) parameter is the most appropriate model for kinetic analysis of $[^{11}C]$GMOM data. The highest baseline K_i values were seen in hippocampus and thalamus, followed by frontal, parietal and occipital cortices, and striatum, and with the lowest values in temporal cortex and cerebellum. This spatial distribution is in line with preclinical results in rat and baboon brain.[13] Furthermore, uptake of $[^{11}C]$GMOM had a spatial distribution that was consistent with the NMDA receptor distribution in postmortem human brain,[25] suggesting preferential uptake in regions with high NMDA receptor density.

A limited number of NMDA receptor ligands have been tested in humans, but they were either inappropriate for imaging purposes or they have not been fully characterized. At present, there appears to be no NMDA receptor tracer that is clearly better than others. The moderate lipophilicity of GMOM

Table 1. Kinetic macro-parameters obtained from fitting the 90 min datasets to the 2T3k_V_B model, together with statistical results from the Wilcoxon signed-rank test with and without the outlier.

Regions	K_i (min^{-1}) mean (SD) Baseline N = 9	S-ketamine N = 6	Statistics P (N = 5)	P (N = 4)	$V_{ND}(K_1/k_2)$ mean (SD) Baseline N = 9	S-ketamine N = 6	Statistics P (N = 5)	P (N = 4)	K_1 (min^{-1}) mean (SD) Baseline N = 9	S-ketamine N = 6	Statistics P (N = 5)	P (N = 4)
Frontal cortex	0.023 (0.014)	0.009 (0.008)	0.14	0.07	8.54 (2.00)	9.33 (1.02)	0.14	0.07	0.48 (0.07)	0.49 (0.08)	0.35	0.47
Temporal cortex	0.020 (0.012)	0.010 (0.012)	0.23	0.07	8.63 (2.06)	9.69 (0.93)	0.08	0.07	0.41 (0.06)	0.42 (0.07)	0.23	0.27
Parietal cortex	0.021 (0.014)	0.008 (0.008)	0.14	0.07	8.81 (1.98)	9.38 (1.20)	0.69	0.47	0.46 (0.05)	0.45 (0.06)	0.89	1.00
Occipital cortex	0.021 (0.012)	0.011 (0.011)	0.14	0.07	8.53 (1.73)	9.24 (1.07)	0.35	0.14	0.47 (0.04)	0.47 (0.06)	0.69	0.72
Cerebellum	0.014 (0.010)	0.005 (0.008)	0.23	0.07	8.43 (2.02)	9.37 (0.98)	0.04	0.07	0.46 (0.07)	0.45 (0.06)	0.89	0.72
Hippocampus	0.028 (0.012)	0.012 (0.013)	0.08	0.07	7.82 (2.25)	9.35 (0.94)	0.04	0.07	0.36 (0.07)	0.37 (0.07)	0.14	0.27
Thalamus	0.024 (0.019)	0.006 (0.007)	0.08	0.07	10.14 (2.56)	11.32 (1.58)	0.23	0.14	0.50 (0.08)	0.52 (0.09)	0.23	0.27
Striatum	0.021 (0.015)	0.007 (0.007)	0.14	0.07	9.15 (1.85)	9.88 (0.86)	0.23	0.07	0.50 (0.06)	0.50 (0.08)	0.69	1.00
Whole brain gray matter	0.021 (0.012)	0.009 (0.010)	0.14	0.07	8.47 (1.88)	9.28 (0.99)	0.14	0.07	0.45 (0.05)	0.45 (0.07)	0.35	0.47
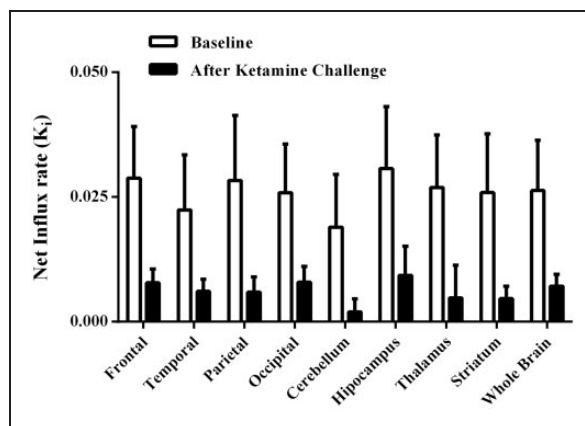
Figure 6. Bar plots (mean with SD error bars) illustrating the effect of S-ketamine on Ki values for all regions of interests investigated. The outlier subject has been excluded for this plot.

(log P = 2.34)[26] is similar to that of [^{11}C]CNS5161 (log P = 1.92),[9] and GE-179 (log $D_{7.4}$ = 2.49).[12] Although [^{11}C]GMOM has a higher affinity (K_d = 5.2 ± 0.3 nM)[26] than [^{11}C]CNS5161 (K_d = 1.9 ± 0.3 nM) and [^{18}F]GE-179 (K_d = 2.4 nM)[12] and the SPECT ligand [^{123}I]CNS1261 (K_d = 4.2 ± 0.4 nM),[9] all suffer from rapid metabolism. Mean parent fractions of [^{11}C]GMOM and [^{18}F]GE-179 are similar with only 50% remaining at 20 min postinjection. In addition, TACs of [^{11}C]GMOM and [^{18}F]GE179 are similar, showing a peak uptake at around 20 min and a prolonged modest decrease until 90 min. However, the rate of metabolism of [^{11}C]GMOM and [^{18}F]GE179 seems to be slower than that of [^{11}C]CNS 5161 and [^{123}I]CNS1261. To examine which tracer is superior, more studies are needed, for example a study that measures the effects of a ketamine challenge for [^{18}F]GE-179 and [^{11}C]CNS 5161.

Pharmacokinetic evaluation indicated that the two-tissue irreversible model with fractional blood volume parameter was the preferred model irrespective of condition (baseline or S-ketamine) or region size, although the preference was more prominent in large regions. From Figure 1, it is more intuitive to consider reversible than an irreversible kinetics. Nevertheless, from the data it seems that GMOM has an irreversible component with very slow kinetics, which is illustrated by high preference for the 2T3k_V_B model based on the AIC comparison. Whole brain TACs together with the best fits obtained using 1T2k_V_B, 2T3k_V_B and 2T4k_V_B models (Supplementary Figure 2) also hint at this preference. Observing the fits it seems that 1T2k_V_B model also fits the data well although considering individual compartments curves (free, nondisplaceable, and specific), particularly 2T3k_V_B, a contribution of irreversible compartment (blue curve in the 2T3k_V_B fit, Supplementary Figure 2) could be seen. The irreversible

specific compartment is very slow but also small. In order words, the curves observed are dominated by the nondisplaceable binding, which has reversible kinetics. In addition, k_3 (using 2T3k_V_B) was estimated reliably. The irreversible model was also able to capture the decrease in net influx rate, K_i, after ketamine challenge. Both k_3 values and the TACs for the irreversible compartment (blue curve in the 2T3k_V_B fit, Supplementary Figure 2) illustrate very slow and small irreversible kinetics of [^{11}C]GMOM. Therefore, it could be anticipated that scans with substantial longer duration than 90 min might indeed have shown an increasing tail in the brain TACs. Moreover, based on the present results a scan duration of at least 90 min is recommended for future [^{11}C]GMOM studies, since there was a shift in model preference with decreasing scan duration indicating that the second tissue compartment only becomes apparent at later (>60 min) scanning times.

As discussed previously and based on previous reports, preference for the irreversible model was not expected.[12,27] A possible explanation for this finding might be the influx of (polar) metabolites into the brain. It is not known whether radiolabelled metabolites of [^{11}C]GMOM are able to cross the blood–brain barrier and enter the brain. Therefore, an additional model including a single tissue compartment for labeled polar metabolites (using the polar metabolites as input function) was investigated. This (dual input) model with blood volume parameter (D1T2k_V_B) used two input functions, one for parent [^{11}C]GMOM, the other for radiolabelled polar metabolites. The model has been described previously by Yaqub et al.[28] with respect to the analysis of dynamic [^{18}F]FDDNP scans. In the present study, the metabolite input function was based on polar metabolites only, thereby ignoring the (small) fraction of nonpolar metabolites. However, this dual plasma input model was not preferred over the standard irreversible model, neither could it detect the expected effects of the S-ketamine challenge (Supplementary Table 1).

Studies have shown a clear association between the affinity of ion-channel blockers for the PCP site and the degree of trapping within the NMDA receptor channel.[29] From a neuropharmacological perspective it is reasonable to assume that a high affinity ligand, such as [^{11}C]GMOM, might stay 90 min or longer at the PCP site of the NMDA receptor, and exhibit irreversible binding during the course of a 90 min PET study.[27,30–32]

K_i values derived from the 2T3k_V_B model were compared between baseline and S-ketamine conditions for all gray matter ROIs included in this study. The expected reduction in tracer accumulation after the S-ketamine challenge was observed at whole brain with high significance and at a trend level in thalamus and hippocampus. It is interesting to note that thalamus and hippocampus are both regions with high NMDA receptor density.[25] In contrast to the other subjects, K_i values in the fifth subject increased after S-ketamine administration, but no reason could be found for this unexpected and counterintuitive result.

No substantial difference in V_{ND} was observed before and after challenge in most ROIs, although a significant increase (nonparametric Wilcoxon signed-rank test) in V_{ND} was found in some ROIs after the challenge. Also no substantial difference in rate constant K_1 was found between pre- and post-S-ketamine administration scans, which indicates that there is almost no change in perfusion and/or extraction due to S-ketamine. However on performing linear mixed model analysis for V_{ND} and K_1, significant but small increases (10% for V_{ND} and 7% for K_1) were found as a result of the challenge. These increases will not affect the conclusion. In fact, it will further support the notion that the significant decrease (linear mixed model analyses) in K_i reflects a decrease of tracer accumulation in the specific compartment (as an increase in K_1 and V_{ND} alone would have resulted in an increase in K_i).

In line with other PET and SPECT ligands of the PCP site,[12,27] [^{11}C]GMOM was metabolized rapidly. As a result, estimation of the polar metabolite fraction was more robust than that of the parent fraction and since the nonpolar metabolite fraction was small, 1 minus the polar fraction was used as a surrogate of the parent fraction. It is possible in case of a very high nonpolar metabolite fraction at earlier time points, that the 1 minus polar fraction would result in a substantial over-estimation of the parent fraction. Supplementary Figure 3 shows that the level of nonpolar metabolites is relatively small at all-time points. Nevertheless, it is also clear that ignoring nonpolar metabolites will result in some bias, which needs to be addressed in future studies. Yet, this study showed that robust plasma input model fits could be obtained and that the effects of the S-ketamine challenge were well captured using plasma input-derived Ki values. An alternative would be a reference model approach but NMDA receptors are important sites of action for glutamate with widespread expression in the whole brain. This is also observed in the present work for all ROI studied. Using in vitro radioligand binding techniques, it has been well established in both rodent[33] and postmortem human[34] brain tissue that there are no regions devoid of NMDA receptors. Therefore, to our best of knowledge, a reference model approach might not be valid for NMDA receptor ligands. Additional limitation of this study is the small sample size and lack of test–retest data. Further studies are needed to assess the within-subject variability in a larger number of subjects.

Conclusion

The plasma input irreversible two-tissue compartment model with additional fractional blood volume is the method of choice for quantification of [^{11}C]GMOM binding, but a scan duration of 90 min or longer is required for robust results. This initial study shows that [^{11}C]GMOM could be used for imaging and quantifying the NMDA receptor.

Declaration of conflicting interests

The author(s) declared no potential conflicts of interest with respect to the research, authorship, and/or publication of this article.

Authors' contributions

TFD: Data acquisition and analysis, drafting, and final approval of the paper. SSVG: Data analysis and interpretation, drafting, and final approval of the paper. PJK: Data acquisition, reviewing, and final approval of the paper. GMOS: Data analysis, reviewing, and final approval of the paper. RCS: Data analysis, reviewing, and final approval of the paper. AM: Study design, reviewing, and final approval of the paper. EJ: Data analysis, reviewing, and final approval of the paper. LAS: Data acquisition, reviewing, and final approval of the paper. ADW Study design, data acquisition, reviewing, and final approval of the paper. AAL: Study design, data interpretation, reviewing, and final approval of the paper. BNMB: Study design, data acquisition, reviewing, and final approval of the paper. RB: Study design, data analysis and interpretation, drafting. and final approval of the paper. TFD and SSVG: contributed equally to this work.

Supplementary material

Supplementary material for this paper can be found at http://jcbfm.sagepub.com/content/by/supplemental-data

References

1. Paoletti P and Neyton J. NMDA receptor subunits: function and pharmacology. *Curr Opin Pharmacol* 2007; 7: 39–47.
2. Sobrio F, Gilbert G, Perrio C, et al. PET and SPECT imaging of the NMDA receptor system: an overview of radiotracer development. *Mini Rev Med Chem* 2010; 10: 870–886.
3. Foster AC and Fagg GE. Neurobiology. Taking apart NMDA receptors. *Nature* 1987; 329: 395–396.
4. White JM and Ryan CF. Pharmacological properties of ketamine. *Drug Alcohol Rev* 1996; 15: 145–155.
5. Carroll RC and Zukin RS. NMDA-receptor trafficking and targeting: implications for synaptic transmission and plasticity. *Trends Neurosci* 2002; 25: 571–577.
6. Coyle JT and Tsai G. NMDA receptor function, neuroplasticity, and the pathophysiology of schizophrenia. *Int Rev Neurobiol* 2004; 59: 491–515.
7. Bossy-Wetzel E, Schwarzenbacher R and Lipton SA. Molecular pathways to neurodegeneration. *Nat Med* 2004; 10: S2–S9.
8. Olivares D, Deshpande VK, Shi Y, et al. N-methyl D-aspartate (NMDA) receptor antagonists and memantine treatment for Alzheimer's disease, vascular dementia and Parkinson's disease. *Curr Alzheimer Res* 2012; 9: 746–758.
9. Robins EG, Zhao Y, Khan I, et al. Synthesis and in vitro evaluation of (18)F-labelled S-fluoroalkyl diarylguanidines: novel high-affinity NMDA receptor antagonists for imaging with PET. *Bioorg Med Chem Lett* 2010; 20: 1749–1751.
10. Waterhouse RN. Imaging the PCP site of the NMDA ion channel. *Nucl Med Biol* 2003; 30: 869–878.
11. Ahmed I, Bose SK, Pavese N, et al. Glutamate NMDA receptor dysregulation in Parkinson's disease with dyskinesias. *Brain* 2011; 134: 979–986.
12. McGinnity CJ, Hammers A, Riano Barros DA, et al. Initial evaluation of 18F-GE-179, a putative PET Tracer for activated N-methyl D-aspartate receptors. *J Nucl Med* 2014; 55: 423–430.
13. Waterhouse RN, Slifstein M, Dumont F, et al. In vivo evaluation of [^{11}C]N-(2-chloro-5-thiomethylphenyl)-N'-(3-methoxy-phenyl)-N'-methylguanid ine ([^{11}C]GMOM) as a potential PET radiotracer for the PCP/NMDA receptor. *Nucl Med Biol* 2004; 31: 939–948.
14. Surti S, Kuhn A, Werner ME, et al. Performance of Philips Gemini TF PET/CT scanner with special consideration for its time-of-flight imaging capabilities. *J Nucl Med* 2007; 48: 471–480.
15. Boellaard R, O'Doherty MJ, Weber WA, et al. FDG PET and PET/CT: EANM procedure guidelines for tumour PET imaging: version 1.0. *Eur J Nucl Med Mol Imaging* 2010; 37: 181–200.
16. van Berckel BN, Oranje B, van Ree JM, et al. The effects of low dose ketamine on sensory gating, neuroendocrine secretion and behavior in healthy human subjects. *Psychopharmacology (Berl)* 1998; 137: 271–281.
17. Vollenweider FX, Vontobel P, Oye I, et al. Effects of (S)-ketamine on striatal dopamine: a [11C]raclopride PET study of a model psychosis in humans. *J Psychiatr Res* 2000; 34: 35–43.
18. Boellaard R, van LA, van Balen SC, et al. Characteristics of a new fully programmable blood sampling device for monitoring blood radioactivity during PET. *Eur J Nucl Med* 2001; 28: 81–89.
19. Lubberink M, Luurtsema G, van Berckel BN, et al. Evaluation of tracer kinetic models for quantification of

P-glycoprotein function using (R)-[11C]verapamil and PET. *J Cereb Blood Flow Metab* 2007; 27: 424–433.

20. Vollmar S, Michel C, Treffert JT, et al. HeinzelCluster: accelerated reconstruction for FORE and OSEM3D. *Phys Med Biol* 2002; 47: 2651–2658.

21. Hammers A, Koepp MJ, Free SL, et al. Implementation and application of a brain template for multiple volumes of interest. *Hum Brain Mapp* 2002; 15: 165–174.

22. Svarer C, Madsen K, Hasselbalch SG, et al. MR-based automatic delineation of volumes of interest in human brain PET images using probability maps. *Neuroimage* 2005; 24: 969–979.

23. Quarantelli M, Berkouk K, Prinster A, et al. Integrated software for the analysis of brain PET/SPECT studies with partial-volume-effect correction. *J Nucl Med* 2004; 45: 192–201.

24. Akaike H. Data analysis by statistical models. *No To Hattatsu* 1992; 24: 127–133.

25. Monaghan DT and Cotman CW. Distribution of N-methyl-D-aspartate-sensitive L-[3H]glutamate-binding sites in rat brain. *J Neurosci* 1985; 5: 2909–2919.

26. Dumont F, Sultana A and Waterhouse RN. Synthesis and in vitro evaluation of N,N′-diphenyl and N-naphthyl-N′-phenylguanidines as N-methyl-D-aspartate receptor ion-channel ligands. *Bioorg Med Chem Lett* 2002; 12: 1583–1586.

27. Erlandsson K, Bressan RA, Mulligan RS, et al. Kinetic modelling of [123I]CNS 1261—a potential SPET tracer for the NMDA receptor. *Nucl Med Biol* 2003; 30: 441–454.

28. Yaqub M, Boellaard R, van Berckel BN, et al. Evaluation of tracer kinetic models for analysis of [18F]FDDNP studies. *Mol Imaging Biol* 2009; 11: 322–333.

29. Mealing GA, Lanthorn TH, Murray CL, et al. Differences in degree of trapping of low-affinity uncompetitive N-methyl-D-aspartic acid receptor antagonists with similar kinetics of block. *J Pharmacol Exp Ther* 1999; 288: 204–210.

30. Keana JF, McBurney RN, Scherz MW, et al. Synthesis and characterization of a series of diarylguanidines that are noncompetitive N-methyl-D-aspartate receptor antagonists with neuroprotective properties. *Proc Natl Acad Sci USA* 1989; 86: 5631–5635.

31. Newman AH. Irreversible ligands as probes for drug receptors. *NIDA Res Monogr* 1991; 112: 256–283.

32. Rafferty MF, Mattson M, Jacobson AE, et al. A specific acylating agent for the [3H]phencyclidine receptors in rat brain. *FEBS Lett* 1985; 181: 318–322.

33. Bresink I, Danysz W, Parsons CG, et al. Different binding affinities of NMDA receptor channel blockers in various brain regions—indication of NMDA receptor heterogeneity. *Neuropharmacology* 1995; 34: 533–540.

34. Quarum ML, Parker JD, Keana JF, et al. (+)-[3H]MK-801 binding sites in postmortem human brain. *J Neurochem* 1990; 54: 1163–1168.